ISBN: 978-3-95450-191-5 doi:10.18429/JACoW-SRF2017-THPB027

CHARACTERIZATION OF MICROSTRUCTURAL DEFECTS IN SRF CAVITY NIOBIUM USING ELECTRON CHANNELING CONTRAST IMAGING

M. Wang, D. Kang, T.R. Bieler, Michigan State University, East Lansing, MI 48824, USA
C. Compton, Facility for Rare Isotope Beams, East Lansing, MI 48824, USA

Abstract

Although the quality factor of niobium cavities has improved, performance variability arises from microstructural defects such as dislocations and grain boundaries that can trap magnetic flux, block heat transfer, and perturb superconducting currents. Microstructural defect evolution is compared in four samples extracted from a 2.8 mm thick large-grain niobium slice, with tensile axes chosen to generate desired dislocation structures during deformation. The four samples are 1) as-extracted, 2) extracted and annealed, 3) extracted and then deformed to 40% strain, and 4) extracted, annealed at 800 ℃ 2 hours, and deformed to 40% strain. Electron channeling contrast imaging (ECCI) was performed on all samples to characterize initial dislocation density, dislocation structure evolution due to annealing and deformation, and related to the mechanical behavior observed in stress-strain curves. Fundamental understanding of dislocation evolution in niobium is necessary to develop computational models to simulate cavity forming.

INTRODUCTION

High purity niobium has been used for the fabrication of superconducting radio frequency (SRF) cavities for decades due to its high critical temperature and good formability [1]. Investigations were carried out to optimize the performance of particle accelerators in different ways, to achieve high accelerating gradient and quality factors. Although great progress has been made to improve the accelerating gradient to a value close to the theoretical limit of niobium, cavity properties still suffer from variability that could be introduced anywhere along the materials processing fabrication path, including ingot remelt, rolling, deep drawing, and electron-beam welding (EBW) [1, 2]. These processing procedures involve plastic deformation that generates microstructural defects such as geometrically necessary dislocations and grain boundaries, which could lead to magnetic flux pinning and residual resistance [2-7].

An anomalous decrease of quality factor with increasing field, also known as Q drop, has been correlated with localized heating during the operation of cavities. The temperature map of the cavity shows hot spots in the high magnetic field regions of the cavity surface, which could be caused by the wiggling of magnetic flux trapped by dislocations and grain boundaries [5]. Low temperature baking eliminates the high field Q drop and reduces surface resistance [8].

† Email: wangmi22@msu.edu

Nevertheless, the relationship between microstructural defects and magnetic field behavior is not very clear, so it is necessary to investigate the dislocation structure evolution in niobium during deformation to understand conditions that may cause flux pinning by dislocations. Once understood, this will guide new processing methods to obtain an optimized microstructure for cavity niobium.

In recent years, large grain or single crystal cavities, which are less expensive and have fewer grain boundaries, have become a new alterative to the traditional fine grain cavities [9, 10]. Studies of slip systems during the deformation of single-crystal niobium have been presented at SRF 2013 and SRF 2015, which shows stress-strain behavior depends strongly on the initial grain orientations and changes resulting from annealing, as well as changes resulting from operation of preferred slip systems during tensile deformation [11, 12]. Better understanding of relationships between crystal orientation, slip systems, and stress-strain behavior are needed for modeling of deep drawing and computational simulation of cavity fabrication that can predict the microstructure and performance of cavities [11, 13].

Direct observation of dislocations in single crystal tensile samples from a previous study was done to build on previous work [11, 12], to enable identification of dislocation character (screw-mixed-edge) and the activity of slip systems underlying the highly orientation dependent stress-strain behavior of single-crystal niobium. This paper focuses on direct observation of dislocation evolution using electron channeling contrast imaging (ECCI), which is a convenient way to observe microstructural defects such as dislocations, stacking faults, nanotwins, and elastic strain fields in bulk materials [14] without destruction of the sample. Details about ECCI can be found in [14-16].

SAMPLE PREPARATION

Four single-crystal niobium samples with the same orientation were extracted from one large grain, and then different processing operations were applied. Sample 1 was as-extracted, Sample 2 extracted and annealed, Sample 3 extracted and deformed to 40% strain, and Sample 4 extracted, annealed at 800℃ for 2 hours, and then deformed to 40% strain. Details of the sample history is found in [11, 12], where crystal rotations indicated predominant slip on {110} planes in the annealed condition, but preferential activity of slip on {112} planes with increasing dislocation density [12].

The samples were then electro-polished in an electrolyte of 90vol% Sulfuric Acid and 10vol%

ISBN: 978-3-95450-191-5 doi:10.18429/JACoW-SRF2017-THPB027

Hydrofluoric Acid using a tungsten cathode while the setup temperature was maintained at -30°C with liquid nitrogen. Electro-polishing was done for 8 minutes under a voltage of 15V, resulting in a mirror-like and scratch free surface.

RESULTS AND DISCUSSION

Bunge's Euler angle system is used to describe the orientation of crystals. Due to the high order of symmetry of the body centered cubic (BCC) crystal structure, there are 24 equivalent Euler angle triplets to describe the same orientation. To reduce confusion, ECC images were taken with the four samples being mounted in the same orientation, using the same crystal coordinate system for ECC image analysis. A MATLAB code was used to calculate all 24 equivalent Euler angle triplets so that the same crystal coordinate system can be chosen.

Indexing of Selected Area Channelling Patterns (SACPs)

In the channeling mode, the MIRA SEM can be used to collect SACPs, which are generated by rocking the electron beam about a chosen spot. The collected SACPs can then be compared with simulated patterns to determine indices of the channeling bands. By tilting and rotating the sample, the primary electron beam center can be moved to the edge of a channeling band to activate a condition analogous to a two-beam condition in transmission electron microscopy, under which the backscattered electron (BSE) image shows enhanced contrast of lattice distortions caused by dislocations.

A prior electron backscattered diffraction (EBSD) scan was used to obtain the Euler angle triplet, which was then used to plot the stereographic projection in Fig. 1a, and to generate simulated SACPs.

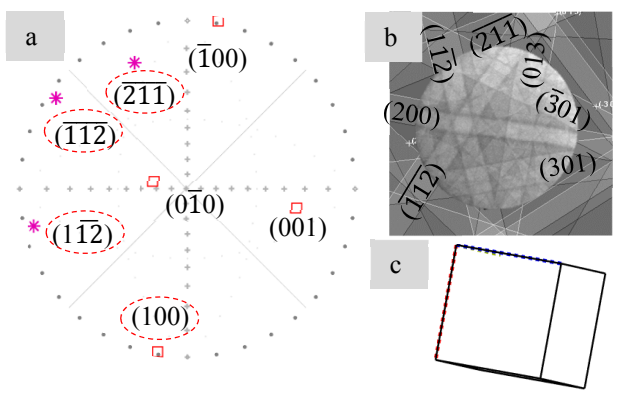

Figure 1: SACP indexing of sample 1 (Euler angles: 170°, 67°, 179°) by overlapping the collected SACP on top of the simulated pattern (b), which is verified by the stereographic projection (a). Indices indicated in (b) are **g** vectors of corresponding channeling conditions and the **g** vectors are perpendicular to the channeling bands. The orientation can also be visualized by a unit cell shown in (c), with red and blue dotted edges representing the x and z axes of the crystal coordinate system, respectively.

TOCA (Tools for Orientation Determination and Crystallographic Analysis) [14, 17, 18] was used to generate simulated SACPs based on the orientation of sample 1 to determine the indices of channeling bands in the collected SACP, as shown in Fig. 1b. The stereographic projection verifies the indexing based on TOCA simulation and the **g** vector indices in Fig. 1b match well with Fig. 1a. Fig. 1c represents the orientation with a unit cell with the red and blue dashed lines representing x and z axes; the y axis points into the page and is not evident in Fig. 1c.

ECCI Observations on Sample 1

ECCI images of the same region were taken under different channeling conditions for the application of $\mathbf{g}\cdot\mathbf{b}$ analysis to identify Burgers vectors of dislocations, as shown in Fig. 2. Dot-like features with dark-light contrast adjacent to each other are threading dislocations that come out of the sample surface. The contrast vector is defined as the direction from the dark end to the light end. Dislocation A is a representative threading dislocation that has a contrast vector (red arrow) perpendicular to the **g** vectors under different channeling conditions, indicating that A is a screw dislocations according to ref [19]. Therefore, A has the same line direction as its Burgers vector and the Burgers vector of A can be identified as $\mathbf{b}=[1\bar{1}1]$, which is close to the direction perpendicular to the sample surface based on the stereographic projection in Fig. 2. This is also confirmed by the $\mathbf{g}\cdot\mathbf{b}$ analysis shown in Table 1. For niobium, there are only <111> dislocations, which are invisible when $\mathbf{g}\cdot\mathbf{b}=0$ and visible otherwise. Both dislocation A and B are visible in the three channeling conditions shown in Fig. 2. In Table 1, all possible Burges vectors are listed and the dot production between **b** and **g** vectors are calculated with plus representing non-zero values and 0 representing zero values.

Table 1: $\mathbf{g}\cdot\mathbf{b}$ Analysis of Sample 1 +: visible 0: invisible

$\mathbf{g}\cdot\mathbf{b}$ analysis		**g** vector		
		(013)	$(\bar{1}\bar{1}2)$	$(\bar{3}01)$
b	[111]	+	+	+
	$[\bar{1}11]$=B	+	+	+
	$[1\bar{1}1]$=A	+	+	+
	$[11\bar{1}]$	+	0	+

Dislocation B appears as a line segment, which is indicated by a black dashed line, as shown in Fig. 2c, and lined up with the [101] direction, meaning B is an edge dislocation because edge dislocations have either <110> or <112> line directions in BCC metals. As a result, the Burgers vector of B can be determined as $\mathbf{b}=[\bar{1}11]$. The $\mathbf{g}\cdot\mathbf{b}$ analysis in Table 1 rules out $[11\bar{1}]$, which should be invisible under $\mathbf{g}=(\bar{1}\bar{1}2)$. The dislocation density is estimated to be 9 μm^{-2} by counting the number of dislocations in in Fig. 3a, which is a zoomed out view of the area in Fig. 2c.

ISBN: 978-3-95450-191-5 doi:10.18429/JACoW-SRF2017-THPB027

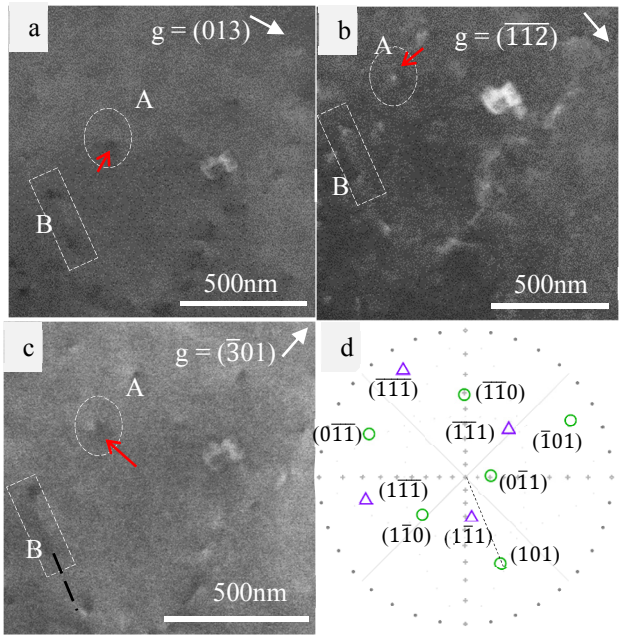

Figure 2: ECC images of Sample 1 under three different channeling conditions (**g** vectors) (a, b, and c) and stereographic projection for the **g**=(3̄01) image (d).

ECCI Observations on Sample 2

Figure 3b shows an ECC image of Sample 2, which was annealed after being extracted. The annealing removes many dislocations and the dislocation density is estimated to be 2 μm^{-2}. This is consistent with the conclusion in the previous research that annealing lowered the flow stress due to removal of pre-existing dislocations [12].

The same methods were applied to identify dislocations in Fig. 3b. According to $\mathbf{g}\cdot\mathbf{b}$ analysis, the Burgers vector of dislocations A, B, C, D, and E should be **b**=[1̄11], which is parallel to the line direction of E, and perpendicular to the line direction of B, making E a screw dislocation and B an edge dislocation. A, C, and D can be identified as mixed dislocations by comparing their line directions with the [1̄11] Burger vector.

ECCI Observations on Sample 3

Sample 3 was extracted and then deformed to 40% strain and the ECC images after deformation (Fig. 4) show tangled dislocation structures, which makes dislocation density estimation difficult, although some of them can be isolated and analyzed.

$\mathbf{g}\cdot\mathbf{b}$ analysis can identify the Burgers vector of dislocation A in Fig. 4a as **b**= [1̄11] , which is perpendicular to the line direction [1̄10] indicated by a black dashed line in the stereographic projection. Therefore, A is an edge dislocation generated on {112} slip systems. Type B in Fig. 4a includes a series of dislocations with line direction parallel to [01̄1], which are edge dislocations generated on {112} slip systems, and the Burgers vectors could be either [1̄11] or [111]. $\mathbf{g}\cdot\mathbf{b}$ analysis is not able to determine the Burgers vector due to image quality issues under other channeling conditions. In this case {112} is the preferred slip system since dislocations of type B are dominant in this region.

Figure 4b shows ECC images of another region of Sample 3. Dislocations C and D have line directions parallel to [2̄11] and [21̄1] respectively, meaning they are both edge dislocations generated on {110} slip systems. This is confirmed by the $\mathbf{g}\cdot\mathbf{b}$ analysis, which identifies the Burgers vectors of C and D as [11̄1] and [111], respectively. The Burgers vectors are perpendicular to the line directions of C and D.

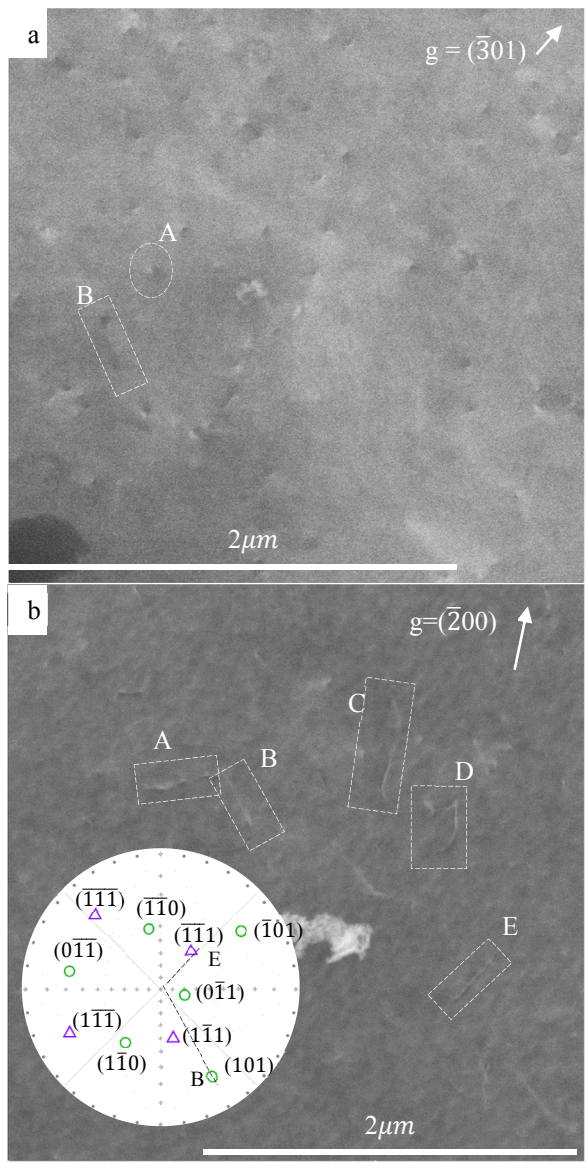

Figure 3: Comparison of ECC images of Sample 1 (a) and Sample 2 (b). Line directions of dislocations B and E are marked in the stereographic projection with black dashed lines.

ECCI Observation of Sample 4

Sample 4 was deformed to 40% strain after being annealed at 800 ℃ for 2 hours and an ECC image is shown in Fig. 5a. Tangled dislocation structures are also

ISBN: 978-3-95450-191-5 doi:10.18429/JACoW-SRF2017-THPB027

observed for Sample 4, and dislocations of type A and B are marked with white dashed arrows and boxes respectively. Type A includes a series of dislocations with line direction parallel to $[0\bar{1}\bar{1}]$ shown in the stereographic projection, which is an edge dislocation line direction from {112} slip systems and the Burgers vector could be either $[\bar{1}\bar{1}1]$ or $[1\bar{1}1]$. Since type A is the dominant dislocations in Fig. 5a, the preferred slip systems should be {112} slip systems. Type B dislocations have a line direction parallel to $[1\bar{1}1]$, which has been identified as the Burgers vector according to $\mathbf{g}\cdot\mathbf{b}$ analysis, indicating that type B are screw dislocations.

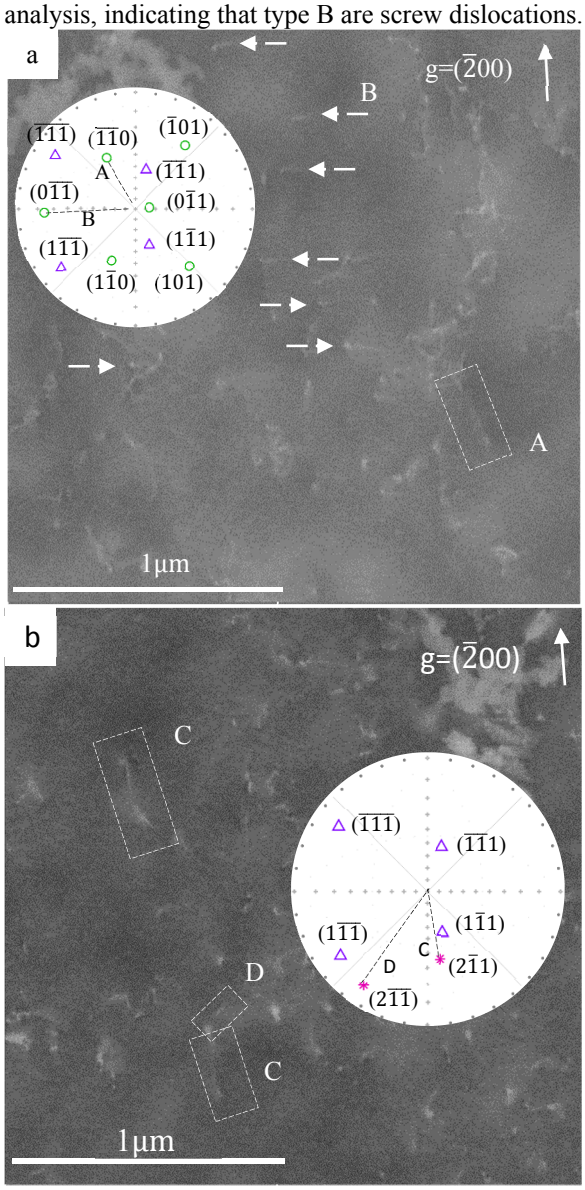

Figure 4: ECC images of two different regions of Sample 3 under the same channeling condition. Dislocation contrast is marked by arrows (a) and boxes (a and b) and the line directions are marked in the stereographic projection by black dashed lines.

Figure 5b shows an ECC image of another region of Sample 4. Dislocations are almost all tangled together and individual dislocation analysis is very difficult. This reflects the 40% deformation that creates many dislocations, which are distributed in a direction that is approximately parallel to the slip traces shown in the second electron (SE) image. The prism in the upper right corner represents the {110} slip system with a slip plane trace having the same direction as the SE image. Therefore, the dislocations in Fig. 5b should be generated by the activation of {110} slip systems.

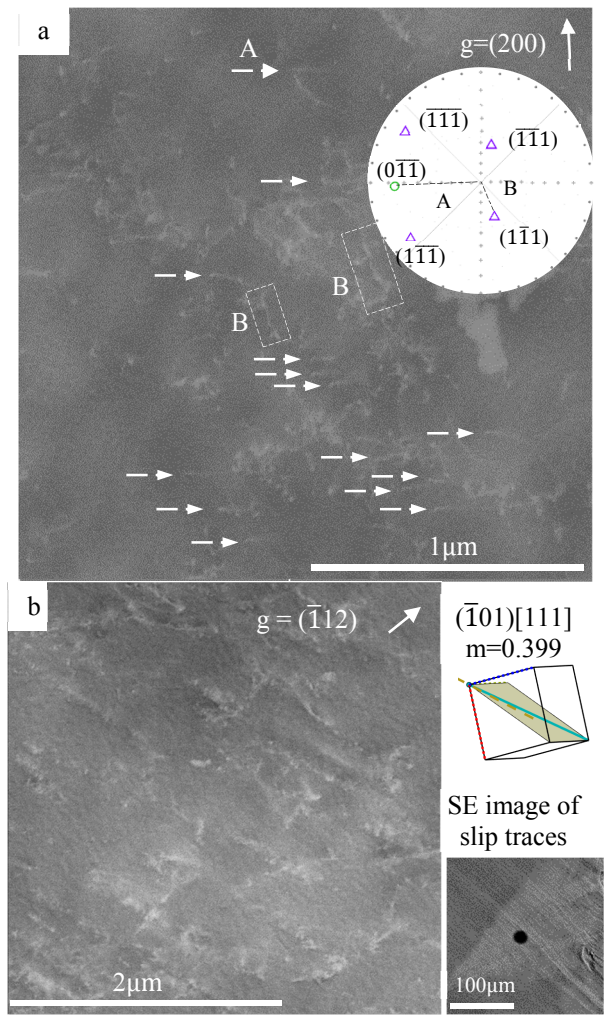

Figure 5: ECC images of two different regions of Sample 4 with dislocations marked by boxes and arrows (a), slip trace image attached (b), and slip system indicated by a prism (b), in which the shaded plane represents the slip plane, the turquoise line shows the Burgers vector, dashed line is the slip trace direction, and m the Schmid factor.

Both {110} and {112} slip systems were observed from the ECC images of Sample 3 that was deformed without annealing, and of Sample 4 that was deformed after annealing. {112} slip systems are found to be the predominant slip systems in both samples, while the previous research [12] pointed out that the annealing changed the preferred slip planes from {112} to {110} based upon a rotation analysis. These observations imply that with increasing strain and dislocation content, the preference for dislocation slip changes from {110} to {112} planes.

ISBN: 978-3-95450-191-5 doi:10.18429/JACoW-SRF2017-THPB027

CONCLUSIONS

Dislocation structures were characterized using ECCI on four single-crystal niobium samples with the same orientation but different heat treatments and deformation history, to identify correlation between stress-strain behavior with the microstructural dislocation structures as well as to identify the dominant slip systems after 40% tensile strain.

For the samples with no deformation, ECCI observations show that the pre-existing dislocation density decreases from 9 μm^{-2} to 2 μm^{-2} due to the 800°C 2-hour annealing, consistent with the flow stress decrease after annealing that was reported in the previous research [12].

Both {110} and {112} slip systems were observed for samples deformed to 40% strain, with the dislocations generated by {112} slip systems being the dominant in the ECC images of both deformed samples 3 and 4. However, the previous research claimed that the preferred slip systems changed from {112} to {110} due to annealing. These two observations can be reconciled if larger levels of strain lead to conditions where slip on {112} planes is favored. Prior observations show slip traces on both planes.

Direct observations of dislocation evolution in this work provides information that can explain observations regarding deformation mechanisms and will be useful for building models for computational cavity design.

ACKNOWLEDGEMENT

Research supported by DOE/OHEP contract DE-SC0009962.

REFERENCES

[1] Singer, W., *SRF Cavity Fabrication and Materials*. arXiv preprint arXiv:1501.07142, 2015.

[2] Bieler, T.R. *et al*., "Physical and mechanical metallurgy of high purity Nb for accelerator cavities". *Physical Review Special Topics - Accelerators and Beams*, p. 031002, 2010.

[3] Ciovati, G. and A. Gurevich. "MEASUREMENT OF RF LOSSES DUE TO TRAPPED FLUX IN A LARGEGRAIN NIOBIUM CAVITY*", in SRF workshop, Beijing, 2007.

[4] Matsushita, T., "Flux pinning in superconductors", *Springer,* vol. 164, New York, 2007.

[5] Ciovati, G. and A. Gurevich, "Evidence of high-field radio-frequency hot spots due to trapped vortices in niobium cavities", *Physical Review Special Topics - Accelerators and Beams*, p. 122001, 2008.

[6] Dasgupta, A. *et al.*, "Flux pinning by grain boundaries in niobium bicrystals", *Philosophical Magazine Part B*, 38(4): pp. 367-380, 1978.

[7] Zerweck, G., "On pinning of superconducting flux lines by grain boundaries", *Journal of Low Temperature Physics*, 42(1-2): pp. 1-9, 1981.

[8] Ciovati, G., "Effect of low-temperature baking on the radio-frequency properties of niobium superconducting cavities for article accelerators", *Journal of Applied Physics*, pp. 1591-1600, 2004.

[9] Kneisel, P. *et al, "*Development of large grain/single crystal niobium cavity technology at Jefferson Lab". in *AIP Conference Proceedings*, pp. 84-97, 2007.

[10] Singer, W. *et al*., "Development of large grain cavities", *Physical Review Special Topics-Accelerators and Beams*, p. 012003, 2013.

[11] Kang, D. *et al*., "Study of slip in high purity single crystal Nb for accelerator cavities", presented at SRF2017, Lanzhou, China, 2017, paper TUP017, this conference.

[12] Kang, D. *et al*. "Study of Slip and Deformation in High Purity Single Crystal Nb for Accelerator Cavities", in *17th International Conference on RF Superconductivity (SRF2015)*, Whistler, BC, Canada, Sept. 2015, pp. 191-195.

[13] Mapar, A. *et al.*, "Dynamic hardening rule; a generalization of the classical hardening rule for crystal plasticity", presented at SRF2017, Lanzhou, China, 2017, paper TUP037, this conference.

[14] Zaefferer, S. and N.-N. Elhami, "Theory and application of electron channelling contrast imaging under controlled diffraction conditions", *Acta Materialia*, 75: pp. 20-50, 2014.

[15] Crimp, M.A., "Scanning electron microscopy imaging of dislocations in bulk materials, using electron channeling contrast", *Microscopy research and technique*, pp. 374-381, 2006.

[16] Kamaladasa, R. and Y. Picard, "Basic principles and application of electron channeling in a scanning electron microscope for dislocation analysis", *Microscopy: science, technology, applications and education*, pp. 1583-1590, 2010.

[17] Zaefferer, S., "New developments of computer-aided crystallographic analysis in transmission electron microscopy", *Journal of Applied Crystallography*, pp. 10-25, 2000.

[18] Zaefferer, S., "Computer-aided crystallographic analysis in the TEM", *Advances in Imaging and Electron Physics*, pp. 355-XII, 2003.

[19] Naresh-Kumar, G. *et al.*, "Rapid nondestructive analysis of threading dislocations in wurtzite materials using the scanning electron microscope", *Physical review letters*, p. 135503, 2012.